Mode selection on breakup of a droplet falling into a miscible solution

Michiko Shimokawa
Fukuoka Institute of Technology, 3-30-1 Wajiro-Higashi, Higashi-ku, Fukuoka 811-0295, Japan

Hidetusgu Sakaguchi
Kyushu University, Kasuga, Fukuoka 816-8580, Japan

(Received 23 March 2017; published 30 January 2019)

When a droplet with a relatively high density falls into a miscible solution with a relatively low density, the droplet breaks up spontaneously. We investigated the number m of breakup in experiments with several density differences $\Delta\rho$ between two solutions, viscosities μ, and droplet radii r. The mode number m has a distribution even under the same experimental conditions. We propose a simple model of mode selection based on the linear Rayleigh-Taylor instability and the growing radius of a vortex ring deformed from the droplet. The model provides the probability distribution $P(m)$ and a relationship between the nondimensional parameter $G \propto \Delta\rho g r^3/\mu^2$ and the average value of m, which are consistent with experimental results.

DOI: 10.1103/PhysRevFluids.4.013603

I. INTRODUCTION

Falling droplets have been a topic of interest within a variety of scientific fields such as physics, mathematics, geoscience, and engineering [1–17]. For example, the breakup of rain droplets was studied by experiments and numerical simulation [1], wherein the surface tension was found to play an important role. On the other hand, when a droplet falls into a miscible viscous fluid without the surface tension (termed the base solution), the droplet deforms into a vortex ring and breaks up due to the instability of that ring [2–7]. The instability of the horizontally moving vortex ring has been studied by many authors [18–25]; however, we consider the instability of the falling vortex ring under the gravity. In the falling process, the shape and velocity of the droplet and the vortex ring change with time; that is, the dynamics are nonstationary, making theoretical analysis difficult.

Arecchi *et al.* focused on (i) the critical condition for the breakup and (ii) the number of breakup. They proposed two kinds of nondimensional parameters $S = \mu/\rho D$ and $F = \Delta\rho g V/\mu D$, where ρ, μ, $\Delta\rho$, g, V, and D are the density of the base solution, the viscosity of the base solution, the density difference between the two solutions, the gravitational acceleration, the volume of the droplet, and the diffusion coefficient, respectively [4,5]. The nondimensional parameter S is the Schmidt number, which indicates the ratio of a viscous effect to a diffusion factor. The nondimensional parameter F is a ratio τ_1/τ_2, where $\tau_1 = r^2/D$ and $\tau_2 = \mu/\Delta\rho g r$ are characteristic timescales of diffusion and a kinetic force due to gravity, respectively. The authors showed the existence of a critical value F_c of F, i.e, there is no breakup for $F < F_c$, but the breakup is observed for $F > F_c$ [4]. They also showed a phase diagram for the number m of breakup in the parameter space of F and S [5]. In our previous paper, we showed that the breakup occurs as a result of the Rayleigh-Taylor instability of the vortex ring formed due to the deformation of the droplet and pointed out the importance of another nondimensional parameter $G = \Delta\rho g r^3 \rho/\mu^2$ [8], where r is the droplet radius when the droplet starts to fall down and G can be expressed by $G = S/F$.

The breakup occurs during the unsteady falling process in which the radius of the vortex ring increases with time. Furthermore, the breakup occurs within a finite time until the droplet falls

down to the bottom of the container. If infinitesimal perturbations are assumed as in the standard linear stability analysis, an infinite period of time would become necessary for the perturbations to grow and the droplet would reach the bottom before ever breaking up; that is, a finite magnitude of perturbations should be considered for the breakup within a finite time of several seconds. In previous papers, the mode selection was considered through dimensional analysis and the comparison between two timescales with respect to the diffusion and the falling droplet [4,5]. In this paper, we focus on the instability of the expanding vortex ring directly, and we show various experimental results and discuss a mechanism of the mode selection under a nonstationary condition during a finite time. Our results would provide a deep understanding of the mode selection of the breakup in the falling process of a droplet.

II. EXPERIMENTAL RESULTS

A. Experimental method

Ferric sulfide aqua solution and glycerine solution were used to produce a relatively heavy droplet solution and a relatively light base solution, respectively. The two solutions are miscible. Ferric sulfide aqua solution was made using ferric sulfide (WAKO 094-01065), water, and polyethylene glycol (PEG; Alfa Aesar B21955). The density difference $\Delta\rho$ is controlled by the ferric sulfide. We had $\rho_1 = 1.18\ \mathrm{g/cm^3}$ and $\rho_2 = 1.12\ \mathrm{g/cm^3}$ in our experiments, where ρ_1 and ρ_2 are densities of the droplet solution and the base solution, respectively. The density difference $\Delta\rho = \rho_1 - \rho_2 = 0.06\ \mathrm{g/cm^3}$ in our experiments is larger than that used in the previous experiment [4,5]. Red food coloring (Kyoritsu Syokuhin) was mixed into the ferric sulfide aqua solution for visualization of droplet deformation. The base solution with the lower density ρ_2 includes glycerine (WAKO 072-00621), water, and PEG. The viscosity μ of the base solution is set to be close to that of the droplet solution by PEG in order to restrict the number of parameters. Figure 1(a) shows μ and ρ_2 for several concentrations x of PEG. As shown in Fig. 1(a), μ increases with x, whereas ρ_2 is independent of x.

Our experimental setup is shown in Fig. 1(b). The radius at the moment when a droplet starts to fall down was controlled using several tubes with different diameters. In our experiments, the radius r was 0.9, 1.1, 1.3, 1.5, and 2.0 mm. A tube is connected to a syringe (TERUMO SS-20ESZ). The syringe is filled with the droplet solution, which is then pushed out using a micro syringe pump (KD Scientific IC3100) at 0.2 μ l/s, as shown in Fig. 1(b). Two types of cylinders were used in our experiments to prevent any influence from the boundary of the cylinder: one was 75 mm in diameter and 145 mm in height, the other was 50 mm in diameter and 260 mm in height. A base solution was poured into one of the cylinders. The cylinder was placed on a horizontal glass table, and the setting made it possible to capture a horizontal deformation of a droplet under the table. A droplet of relatively high density was caused to fall from $h = 8.0$ mm, where $h = 0$ indicates the position of the surface, and sinks into a base solution. The behavior was captured from the side and the bottom of the cylinder using video cameras, whose positions are shown as Camera 1 and Camera 2 in Fig. 1(b). The obtained movies illustrated the vertical and the horizontal deformation processes of the droplet and were analyzed using an image processing system (ImageJ, Nature Institutes of Health, USA).

B. Probability distribution of breakup number *m*

When a droplet falls into a miscible viscous fluid, it spontaneously breaks up according to the following process [4,5,8]: (1) the spherical droplet deforms into a flat pancake shape, (2) a hole is created at its center and a vortex ring is formed, (3) the vortex ring expands in a radial direction, and (4) the vortex ring deforms and is broken into several droplets. Breakups of $2 \leqslant m \leqslant 8$ were observed in our experiments, where m is the breakup number.

Figure 2 shows snapshots of the droplet deformation, captured from the position of Camera 2 shown in Fig. 1(b). The deformation of a droplet was observed after the vortex ring formation. The droplet deforms to polygons such as (b) a triangle for $m = 3$, (c) a square for $m = 4$, and

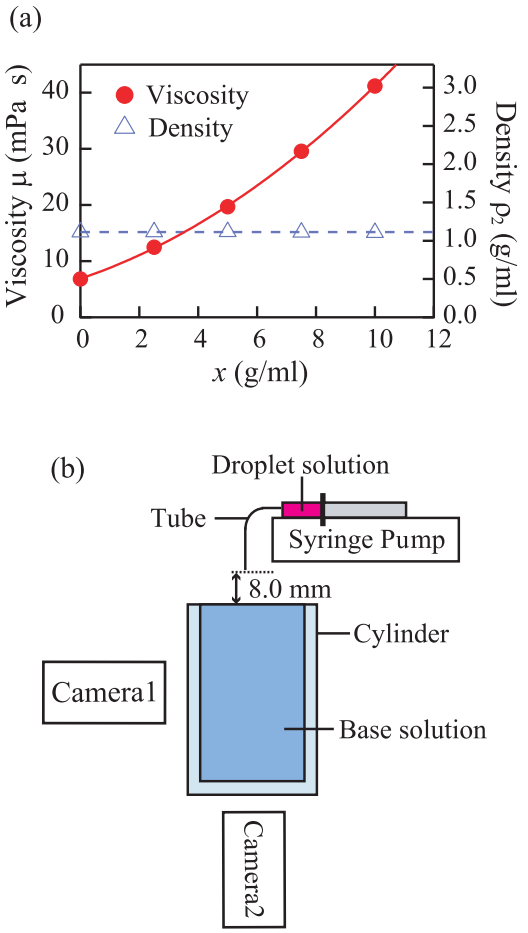

FIG. 1. (a) Viscosity μ and density ρ_2 of the base solution for several concentrations x of PEG. (b) Experimental setup.

(d) a pentagon for $m = 5$. Heavier solution concentrates at the vertices of the polygons and daughter droplets are generated.

We experimentally investigated the probability distribution $P(m) = n(m)/N$. Here $n(m)$ is the number of experiments in which mode number m was obtained and $N = 50$ is the total number of

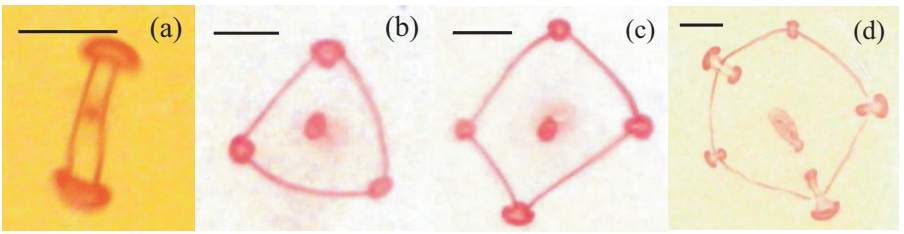

FIG. 2. Droplet deformation with (a) a digon shape, (b) a triangular shape, (c) a square shape, and (d) a pentagonal shape, as captured from the bottom of a beaker. Solid lines in the photos show 5.0 mm scale bars.

experiments. We confirmed that the shape of distribution converged with the data with $N > 30$ in our experiments. Thus, we regarded that $N = 50$ was a satisfied value in the measurements of $P(m)$.

We investigated the dependence of $P(m)$ in experiments with several initial radii r of the droplet. The viscosities of the two solutions were kept constant at $\mu = 10.2$ mPa · s, and the density difference was also kept constant at $\Delta\rho = 0.06$ g/cm^3. Figure 3 shows the results in experiments with (a) $r = 0.9$ mm, (b) 1.1 mm, (c) 1.3 mm, (d) 1.5 mm, and (e) 2.0 mm. The selected modes m were distributed as shown in Fig. 3 with the same experimental conditions. The peak positions of $P(m)$ are $m = 2$ for $r = 0.9$ mm [Fig. 3(a)], $m = 3$ for $r = 1.1$ mm [Fig. 3(b)], $m = 4$ for $r = 1.3$ mm and 1.5 mm [Figs. 3(c) and 3(d), respectively], and $m = 5$ for $r = 2.0$ mm [Fig. 3(e)]. This result indicates that the selected mode m increases with the radius r of the droplet. It is also supported by a comparison of Fig. 3(c) with Fig. 3(d), showing that the distribution shifts toward the larger mode, although the peak position $m = 4$ in Fig. 3(c) is similar to that in Fig. 3(d).

We also investigated the viscous dependence of $P(m)$ obtained from experiments with $r = 1.5$ mm, and $\Delta\rho = 0.06$ g/cm^3. Figure 4 shows the results for experiments with (a) $\mu =$ 7.2 mPa · s, (b) 10.2 mPa · s, (c) 15.2 mPa · s, and (d) 18.2 mPa · s. As shown in Fig. 4, the peak positions of $P(m)$ were $m = 4$ for 7.2 mPa · s and 10.2 mPa · s [Figs. 4(a) and 4(b), respectively], $m = 3$ for 15.2 mPa · s [Fig. 4 (c)], and $m = 2$ for 18.2 mPa · s [Fig. 4(d)]. This result indicates that the selected mode m decreases with the viscosity μ of the solution. In addition, our experimental results showed a tendency that m increased with $\Delta\rho$. This result is able to be confirmed in Fig. 5(b).

C. Relationship between m and G

In the previous paper, we proposed the following equations and performed numerical simulations of a falling vortex ring [8]:

$$\frac{\partial \mathbf{u}}{\partial t} + \mathbf{u}\cdot\nabla\mathbf{u} = -\frac{1}{\rho_2}\nabla P + \nu\nabla^2\mathbf{u} - \frac{\rho-\rho_2}{\rho_2}g\mathbf{e}_z, \tag{1}$$

$$\frac{\partial \rho}{\partial t} + \mathbf{u}\cdot\nabla\rho = D\nabla^2\rho, \tag{2}$$

where $\mathbf{u}$, ρ, ρ_2, ν, P, and D are the flow velocity, density of solution, density of the base solution, kinematic viscosity μ/ρ_2, pressure, and a diffusion coefficient, respectively. Equation (1) is the Navier-Stokes equation for the fluid with inhomogeneous density. Equation (2) is the advection-diffusion equation for the density. Dimensionless equations are obtained by the scale transformation; $x' = x/r$, $u' = ur/\nu$, $t' = t\nu/r^2$, $P' = Pr^2/\rho_2\nu^2$, $\rho' = (\rho-\rho_2)/\rho_2$:

$$\frac{\partial \mathbf{u}'}{\partial t'} + \mathbf{u}'\cdot\nabla'\mathbf{u}' = -\nabla' P' + u\nabla'^2\mathbf{u}' - G\rho'\mathbf{e}_z, \tag{3}$$

$$\frac{\partial \rho'}{\partial t'} + \mathbf{u}'\cdot\nabla'\rho' = \frac{1}{S}\nabla'^2\rho', \tag{4}$$

where $S = \nu/D$ and $G = (\rho_1-\rho_2)/\rho_2(gr^3/\nu^2)$, and ρ_1 is the initial density of the droplet. The term G can be expressed as S/F, where the parameters F and S were proposed by Arecchi *et al.* [4,5].

We investigated the dependence of mode m on several values of G and S. We could not measure the diffusion coefficient D directly, although D is included in the calculation of S. Instead, we considered that the diffusion of $Fe_2(SO_4)_3$ in a droplet plays an important role and evaluated this using the Einstein-Stokes law and data relating to ionic diffusion coefficients [9]. Reference [9] shows the diffusion coefficient $D_{H2O} \sim 8.16\times10^{-10}$ m^2/s for $Fe_2(SO_4)_3$ in H_2O at 25. As D is proportional to μ^{-1} by the Einstein-Stokes law, $D(\mu) = (\mu_{H2O}/\mu)D_{H2O}$. Substitution of $\mu_{H2O} =$ 0.89 mPa · s provides $D(\mu) = 7.26\times10^{-13}/\mu$ (m^2/s). S can be estimated from $D(\mu)$.

Figure 5(a) shows a phase diagram of breakup number m. The horizontal and vertical axes represent S and G, respectively. The average value $\langle m\rangle$ is calculated using $P(m)$. In this phase diagram, m is set to 2 for $2 \leqslant \langle m\rangle < 3$, 3 for $3 \leqslant \langle m\rangle < 4$, and 4 for $4 \leqslant \langle m\rangle < 5$. The parameter

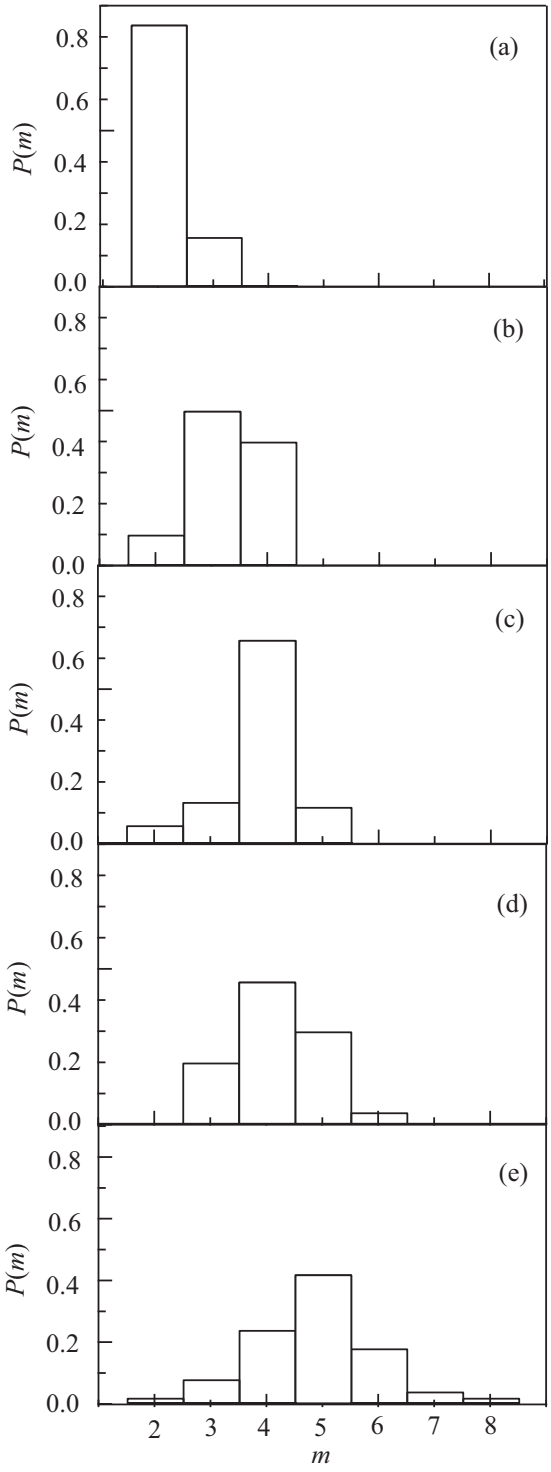

FIG. 3. Probability distributions $P(m)$ for mode m obtained from experiments with several droplet radii (a) $r = 0.9$ mm, (b) 1.1 mm, (c) 1.3 mm, (d) 1.5 mm, and (e) 2.0 mm when a droplet starts to fall. The density difference between two solutions is 0.06 g/cm^3, and viscosities of two solutions are 10.2 mPa · s.

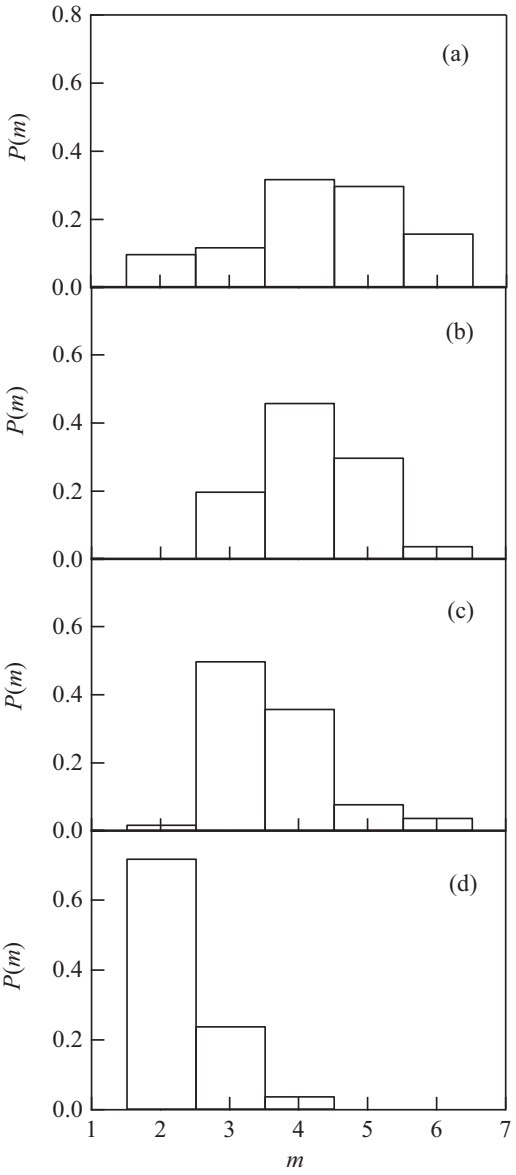

FIG. 4. Probability distributions $P(m)$ for mode m obtained from experiments with several viscosities (a) $\mu = 7.2$ mPa · s, (b) 10.2 mPa · s, (c) 15.2 mPa · s, and (d) 18.2 mPa · s. Density difference 0.06 g/cm^3 between two solutions and droplet radius 1.5 mm at the time when a droplet started to fall down were kept constant in the measurements.

values for $m = 2,\ 3$, and 4 are plotted with closed circles, open triangles, and closed squares, respectively. As shown in Fig. 5(a), $\langle m \rangle$ depends on G, but hardly depends on S for $4.0 \times 10^4 \leqslant S < 1.0 \times 10^6$. This result implies that (i) the diffusion does not have an influence over the mode selection of the breakup and (ii) G is an important parameter for the mode selection. Result (i) is different from previous studies [5,7]. As for the reason, it is considered that the density difference of 10^{-2} g/cm^3 in our experiments is larger than the 10^{-6}–10^{-5} g/cm^3 in previous studies.

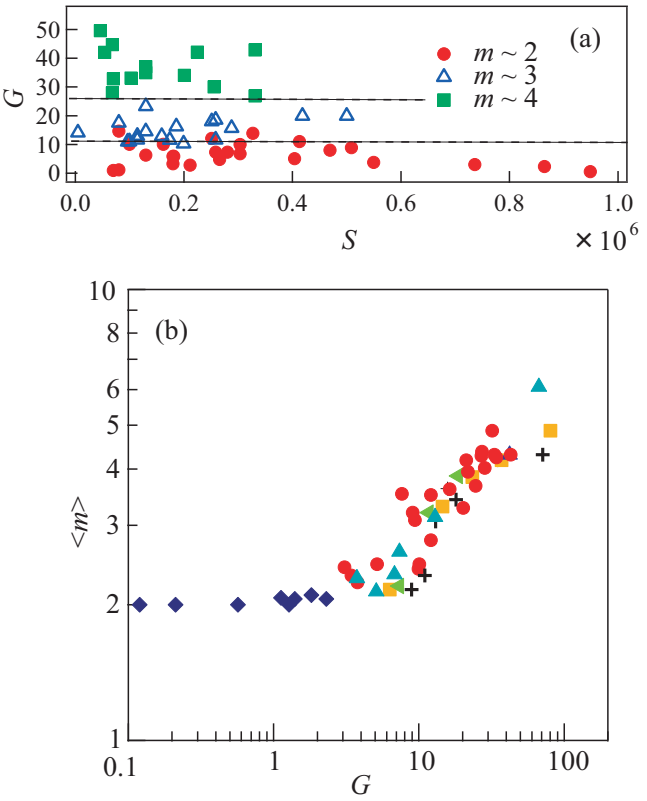

FIG. 5. (a) Phase diagram of breakup mode m obtained from probability distribution in experiments with several density differences, viscosities, and droplet radii. (b) Relationship between G and $\langle m \rangle$ in a logarithmic scale. The parameters for each marker are as follows: $\Delta\rho = \rho_1 - \rho_2 = 0.25$ g/cm^3 and $r = 0.9$ mm for closed triangles; $\Delta\rho = 0.06$ g/cm^3 and $r = 1.5$ mm for asterisks; $\Delta\rho = 0.06$ g/cm^3 and viscosity $\mu = 10.2$ mPa · s for closed squares; and $\Delta\rho = 0.06$ g/cm^3 and viscosity $\mu = 14.4$ mPa · s for inclined closed triangles. Data obtained from experiments with several density differences are shown as closed diamonds.

Next, we investigated a relationship between G and $\langle m \rangle$. Figure 5(b) shows $\langle m \rangle$ for various values of G, which are obtained for various viscosities μ, density differences $\Delta\rho$, and droplet radii r. The average value $\langle m \rangle$ increases with G at $G \gtrsim 4$, and $\langle m \rangle$ has close to 2 at $G \lesssim 4$. The data suggest the existence of a scaling law of $\langle m \rangle$ as a function of G at $G \gtrsim 4$.

III. THEORETICAL ARGUMENTS

In the previous paper, we showed that the thickness d of the vortex ring decreases at the early stage because the vortex ring expands, however, the vortex ring deforms vertically owing to the Rayleigh-Taylor instability. As a result, there is a critical time t_c when the effective thickness d takes the minimum d_c. We found that the relationship between the thickness and the wavelength of the deformation at $t = t_c$ is in good agreement with that between the thickness and the most unstable wavelength for the Rayleigh-Taylor instability of two-layer fluids [8].

We extend the argument for the mode selection of the breakup of a vortex ring. The linear growth rate $s(k)$ for the sinusoidal perturbation of wave number k on two-layer fluids can be calculated using the method of Chandrasekhar [17]. The thickness of the upper layer is assumed to be d and that of the lower layer is infinite. Figure 6(a) shows the relationship between k and $s(k)$ for $d = 0.1$, $\rho_1 = 1.2$, $\rho_2 = 1.1$, $g = 980$, and $\nu = 0.1$. Here the cgs system of units is used. Note that the maximum

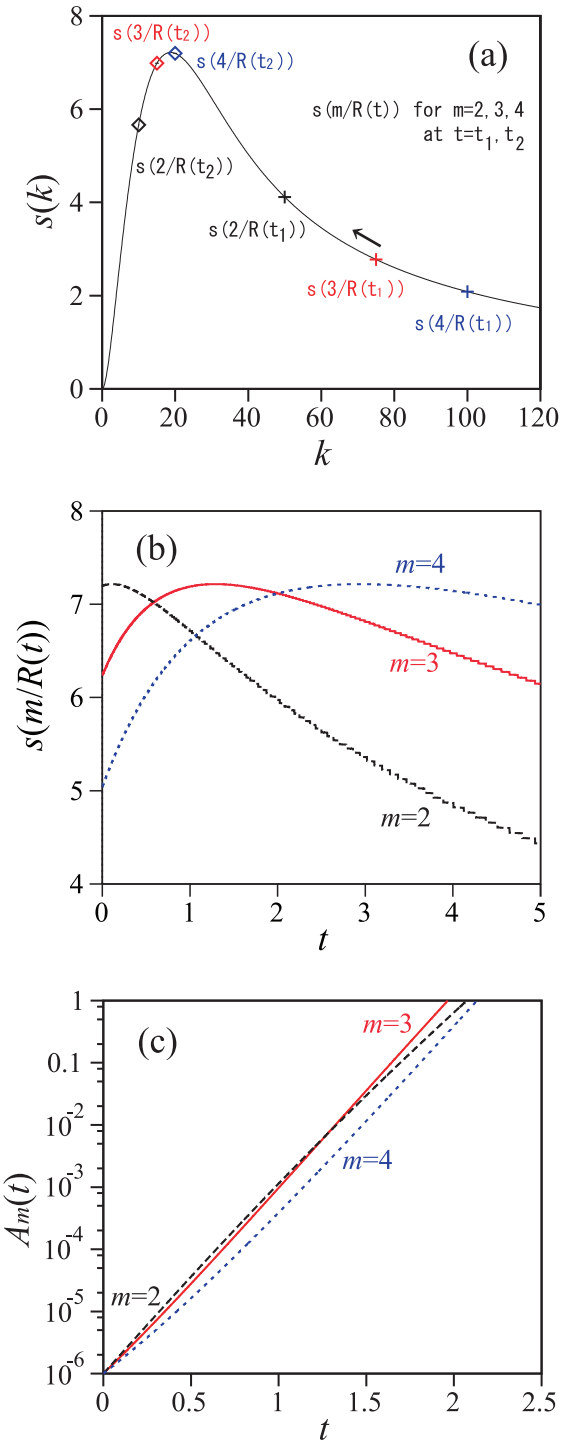

FIG. 6. (a) Linear growth rate $s(k)$ of the Rayleigh-Taylor instability for $d_c = 0.1$, $\rho_1 = 1.2$, $\rho_2 = 1.1$, $g = 980$, and $\nu = 0.1$. (b) Time evolution of $s(k) = s(m/R(t))$ for $m = 2$ (dashed line), $m = 3$ (solid line), and $m = 4$ (dotted line). (c) Time evolutions of perturbation $A_m(t)$ for $m = 2$ (dashed line), $m = 3$ (solid line), and $m = 4$ (dotted line) in a semilogarithmic scale.

growth rate is about 7, which implies that an initial perturbation of $e^{-7} \sim 0.00091$ grows to 1 for $\Delta t = 1$s. On the other hand, Turner showed that the radius of a vortex ring increases under the gravity [26] as

$$R(t) = \sqrt{R(0)^2 + \alpha t}, \tag{5}$$

where $\alpha = gV\Delta\rho/(\pi\rho\Gamma)$, V is the volume of the vortex ring, and Γ is the circulation of the vortex ring.

We consider the Rayleigh-Taylor instability on such an expanding vortex ring. For the mode number m, the wave number k is expressed as $k(t) = 2\pi/\lambda = 2\pi/(2\pi R(t)/m) = m/R(t)$. Since $R(t)$ increases as $R(t) = \sqrt{R(0)^2 + \alpha t}$, the growth rate $s(k) = s(m/R(t))$ obtained from Rayleigh-Taylor instability changes with time as shown in Fig. 6(b). Then the perturbation $A_m(t)$ of mode m is expected to grow as

$$A_m(t) = A_m(0)\exp\left\{\int_0^t s(k)\,dt\right\} = A_m(0)\exp\left\{\int_0^t s(m/\sqrt{R(0)^2 + \alpha t})\,dt\right\},$$

where $A_m(0)$ is the initial value of $A_m(t)$. The initial values are assumed to be the same $A_m(0) = 10^{-6}$, $R(0) = 0.1$, and α is set to 0.012. The other parameters are the ones used in Fig. 6(a).

Figure 6(c) shows the time evolutions of $A_m(t)$ for $m = 2,\ 3$, and 4 in a semilogarithmic scale. The behavior of $A_m(t)$ is not simple, because $s(m/R(t))$ changes with time as shown in Fig. 6(b). In Fig. 6(a) the linear growth rate $s(m/R(t))$ for $m = 2,\ 3$, and 4 at $t = t_1$, and t_2 are plotted as examples, where $t_1 < t_2$. Initially, $A_2(t)$ increases most rapidly, because the effective wave number $k = m/R(t)$ is the smallest for $m = 2$ and all wave numbers are located in the right region of the peak position of $s(k)$ in Fig. 6(a). However, the effective wave number $k(t) = m/R(t)$ decreases with time and the wave number becomes smaller than the wave number corresponding to the peak position of $s(k)$, then $s(m/R(t))$ for $m = 2$ becomes smaller than that for $m = 3$ or 4 as shown in Fig. 6(b). As a result, the order of $A_m(t)$ can be changed. We assume that the mode m whose $A_m(t)$ reaches first the goal value 1 wins the mode-selection race and is selected. That is, we speculate from the experimental results that nonlinear dynamics become dominant and a come-from-behind victory does not occur after that. The perturbation A_m of the selected mode develops further in the falling process, which leads to the breakup of the droplet. The number of the secondary droplets is equal to the selected mode number m. In this case, mode 3 reaches first 1, mode 2 second, and mode 4 the last as shown in Fig. 6(c), and then mode 3 is selected. The goal value is set to 1 in our model, since the nonlinear effect is expected to become dominant for $A_m(t) > 1$; however, the magnitude of the goal value is not important because only the total amplification factor $A_m(t)/A_m(0)$ is meaningful in the linear growth process.

Which mode is selected depends on the initial value $A_m(0)$ and the parameter α of the expansion. As $A_m(0)$ is smaller, the time necessary to reach the goal value 1 is longer, and then the vortex ring becomes larger, as a result, a larger m is selected. As α is larger, the vortex ring expands quickly, and then a larger m tends to be selected. Figure 7(a) shows that the selected mode number m as α is changed for $A_m(0) = 10^{-6}$ and $R(0) = 0.1$. The selected mode increases stepwise with α.

Next, we expect that the initial values $A_m(0)$ are randomly distributed, although the origin of the randomness is not well understood. They might be fluctuating owing to thermal noises or some fluctuations might be excited when the droplet falls into the base solution. In any cases, we can calculate the probability distribution $P(m)$ of selected mode m from the random initial conditions of $A_m(0)$. Figure 7(b) shows $P(m)$ when $A_m(0)$ obeys the Gaussian distribution of standard deviation of 10^{-6} for $R(0) = 0.1$ and $\alpha = 0.04$. The selected mode is distributed. The peak mode number is 4; however, the other modes such as $m = 3,\ 5$, and 6 also appear. The wide probability distribution of experimentally obtained mode number shown in Figs. 3 and 4 can be interpreted by this mechanism.

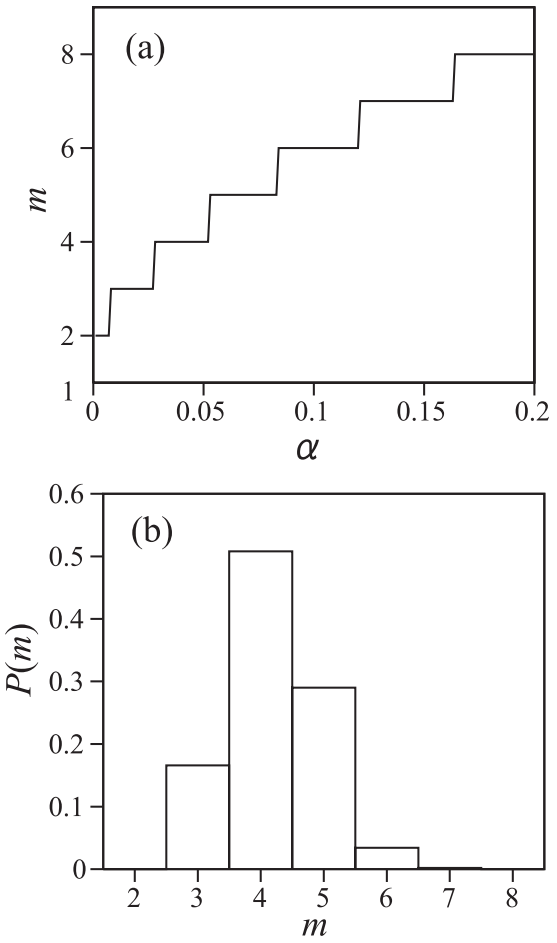

FIG. 7. (a) Selected mode m as a function of α for $A_m(0) = 10^{-6}$ and $R(0) = 0.1$. (b) Probability distribution $P(m)$ of selected mode when $A_m(0)$ obeys the Gaussian distribution of standard deviation of 10^{-6} for $R(0) = 0.1$ and $\alpha = 0.04$.

IV. COMPARISON BETWEEN EXPERIMENTAL RESULTS AND THEORETICAL ARGUMENTS

In this section, we compare the experimental results with theoretical arguments. First, we measured the time dependences of the vortex ring radius $R(t)$ to estimate the α values from experiments. The shape of the droplet keeps the sphere shape at $t \lesssim t_0$, and the droplet begins to deform to a vortex ring at a time t_0 after a droplet starts falling. The times t_0 are 0.23 s for $\mu = 10.2$ mPa · s, 0.36 s for 15.2 mPa · s, and 0.9 s for 20.2 mPa · s, respectively. We investigated $R^2(t') - R^2(0)$ using the measurements of $R(t')$, where $t' = t - t_0$. Figure 8 shows the data for $\mu = 10.2$ mPa · s as open circles, for 15.2 mPa · s as open squares, and 20.2 mPa · s as open triangles with a constant value of a droplet radius $r = 1.5$ mm. The data increase close to linear at $0 < t' < t_c - t_0$.

From the slope of the linear fitting, α is evaluated, which is a parameter characterizing the expanding speed of the vortex ring. This data show that α decreases with the viscosity as shown in Fig. 8; that is, the α decreases with m, since the values m of these data for $\mu = 10.2$ mPa · s, 15.2 mPa · s, and 20.2 mPa · s are 4, 3, and 2. The results show a similar tendency to the consideration shown in Sec. III.

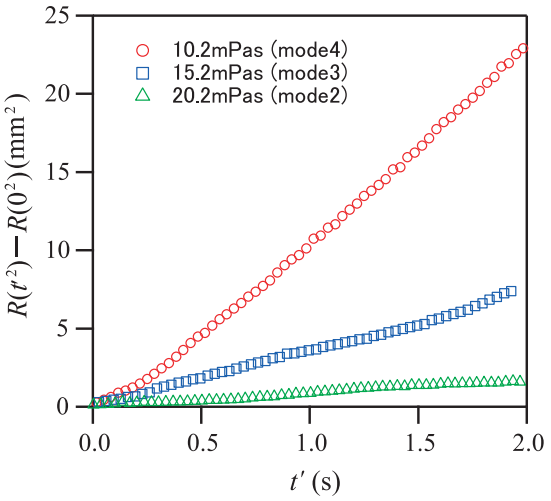

FIG. 8. Plots of $R^2(t') - R^2(0)$ for the evaluation of the α value, where $t' = 0$ is a time when the deformation of the vortex ring becomes visible. Data of circles, squares, and triangles are obtained from experiments of $\mu = 10.2$ mPa · s ($m = 4$), 15.2 mPa · s ($m = 3$), and 20.2 mPa · s ($m = 2$), respectively. The radius of a droplet 1.5 mm was kept constant in those experiments.

From α, another nondimensional parameter α/ν is obtained. If the dynamics of a falling droplet can be expressed with Eqs. (3) and (4) and the effect of diffusion in Eq. (4) is negligible ($S = \infty$), the only important nondimensional parameter is G. The droplet changes into a vortex ring in the falling process owing to the Kelvin-Helmholtz instability, and the nondimensional parameter α/ν is expected to be closely related to the nondimensional parameter G. Figure 9 shows a relationship between G and α/ν for various values of r for $\mu = 10.2$ mPa · s (circles) and those of μ for $r = 1.5$ mm (squares). A linear relation of $\alpha/\nu = a_1 G + a_2$ is approximately satisfied, where $a_1 = 4.30 \times 10^{-2} \pm 0.44 \times 10^{-2}$ and $a_2 = -15.99 \times 10^{-2} \pm 6.04 \times 10^{-2}$.

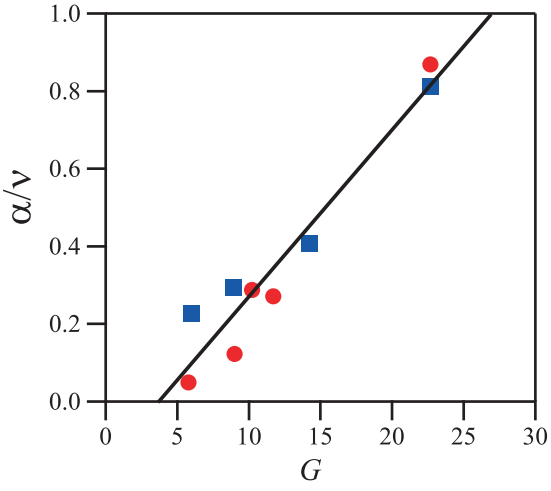

FIG. 9. Relationship between α/ν and G for various values of r for $\mu = 10.2$ mPa · s (circles) and those of μ for $r = 1.5$ mm (squares). The linear line denotes $\alpha/\nu = a_1 G + a_2$, where $a_1 = 4.30 \times 10^{-2} \pm 0.44 \times 10^{-2}$ and $a_2 = -15.99 \times 10^{-2} \pm 6.04 \times 10^{-2}$.

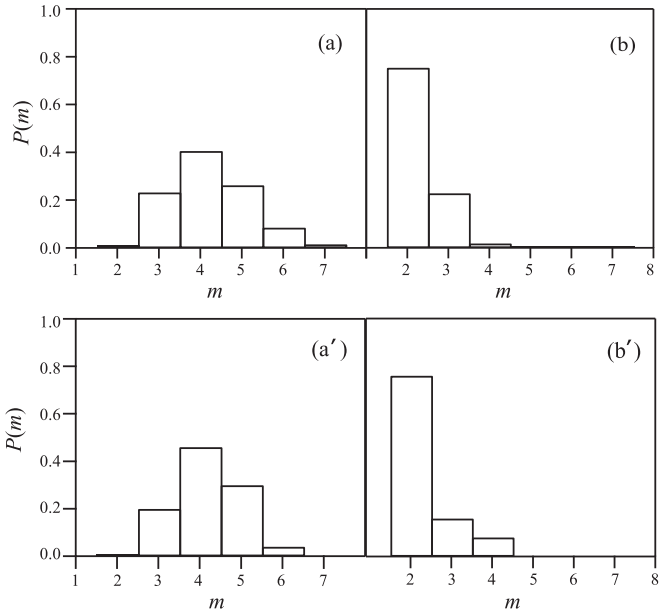

FIG. 10. Probability distributions $P(m)$ of selected mode number. The upper row shows numerical results for (a) $\nu = 0.0911$ and (b) 0.145. The lower row shows experimental results for (a′) $\nu = 0.0911$ and (b′) 0.145 with a droplet radius $r = 1.5$ mm.

From this relation, α is predicted from G. The linear growth rate as shown in Fig. 6 is determined by G. In the evaluation of the linear growth rate, the height $H(t)$ of the vortex ring is calculated using the conservation law of the volume $\pi^2 R(t)H(t)^2/2$ of the vortex ring (torus), and the thickness d of the heavier fluid layer is assumed to be equal to $H(t)$. The mode number can be calculated using the method of the previous section if the initial conditions $A_m(0)$ are known; however, they are too small to evaluate in experiments. Instead, we can estimate the critical time $t_c' = t_c - t_0$ obtained in experiments, when the deformation of the vortex ring becomes visible, from the observation of the thickness of the vortex ring [8]. We interpret that the time t_c' is the goal time when $A_m(t)$ reaches 1. The goal time t_c' depends on the initial value $A_m(0)$. Using the critical time t_c', $A_m(0)$ is evaluated as the order of 10^{-3}–10^{-4}. We have estimated that the probability distributions of initial values of $A_m(0)$ obey Gaussian distributions of standard deviation of $10^{-3.5}e^{-0.015m^2}$ from the comparison between experimentally observed probability distributions of selected mode number and numerically obtained ones. Figure 10 shows theoretically estimated probability distributions $P(m)$ [(a) and (b)] and experimentally obtained $P(m)$ [(a′) and (b′)] for two parameter values of $\nu = 0.0911$ and 0.145 with $\Delta\rho = 0.06$ and $\rho_2 = 1.12$. The critical times t_c' s are 1.7 s and 2.0 s in Figs. 10(a) and 10(b) obtained from numerical results, whose values are close to experimental values of 1.70 s and 2.67 s in Figs. 10(a′) and 10(b′). Fairly good agreement is seen between experimental and numerical results.

Furthermore, we have calculated the average value $\langle m \rangle$ for various values of G by using the linear relation α/ν and the Gaussian distribution of standard deviation $10^{-3.5}e^{-0.015m^2}$ for the initial values of $A_m(0)$, where the parameter values -3.5 and -0.015 are obtained from the fitting with the experimental data of Fig. 10(a′). Figure 11 compares the experimental results (circles) shown in Fig. 5 with the numerical results (line). Fairly good agreement is seen, although numerical results are based on various assumptions and rough approximations.

Our experiments focus on an experimental condition of $\rho_1 > \rho_2$ in this paper, where ρ_1 and ρ_2 are densities of a droplet solution and a base solution. Even for negative density difference $\rho_1 < \rho_2$

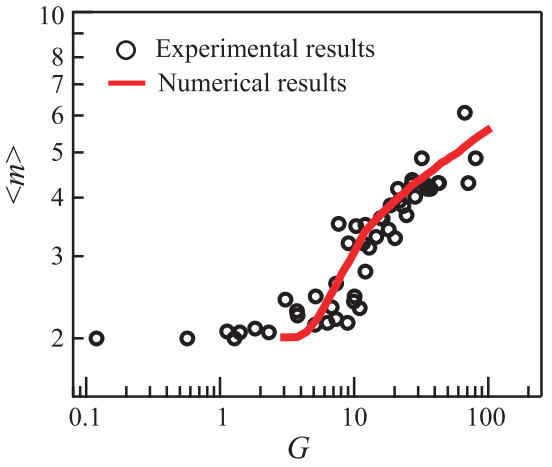

FIG. 11. Relationship between G and $\langle m \rangle$. Experimental results are denoted by marks and the numerical results are denoted by a solid curve [27].

[21] and zero density difference $\rho_1 \sim \rho_2$ [20], we expect that the figures corresponding to Figs. 10 and 11 could be plotted, if we could know the relationship between G and α/ν such as Fig. 9; however, this is left for the future.

V. SUMMARY

When a droplet with a relatively high density falls into a miscible solution with a relatively low density, the spontaneous breakup occurs. To understand a mechanism of the mode selection, the breakup number was investigated in experiments with various viscosities, together with various droplet radii and several density differences between the two solutions. We have found that the selected mode number is not uniquely determined for the same experimental setup and measured the probability distributions $P(m)$ of selected mode number m. We also have found that the average value $\langle m \rangle$ of the selected mode is determined almost only by the nondimensional parameter G.

We have proposed a mechanism of the mode selection based on the Rayleigh-Taylor instability of the expanding vortex ring. A finite magnitude of initial perturbations is necessary for the deformation of the vortex ring to grow in a finite time around several seconds until the falling droplet reaches the bottom of beakers. Our problem is a problem of finite-time instability of a nonstationary state. By assuming Gaussian distributions for initial perturbations whose magnitudes are consistent with the critical time of deformation of vortex rings, we have obtained the probability distributions $P(m)$ and a relationship between G and $\langle m \rangle$. These results are in fairly good agreements with experimental results.

ACKNOWLEDGMENTS

We would like to thank Prof. M. Tokita, Prof. H. Honjo, and Prof. S. Ohta at Kyushu University, Prof. T. Takami at Oita University, T. Nakajima at Fukuoka Institute of technology for their fruitful discussions and suggestions. M.S. would like to thank Samantha Hawkins of the Fukuoka Institute of Technology for proofreading this manuscript. This work is supported by JSPS KAKENHI Grants No. 15K17723 and 18K03462, and the Electronics Laboratory at the Fukuoka Institute of Technology.

[1] E. Villermaux and B. Bossa, Size distribution of raindrops, Nat. Phys. **6**, 232 (2010).
[2] J. J. Thomson and H. F. Newall, V. On the formation of vortex rings by drops falling into liquids, and some allied phenomena, Proc. R. Soc. London **39**, 417 (1885).
[3] D. W. Thompson, *On Growth and Form* (Cambridge University Press, Cambridge, 2001).
[4] F. T. Arecchi, P. K. Buah-Bassuah, F. Francini, C. Perez-Garcia, and F. Quercioli, An experimental investigation of the break-up of a liquid drop falling in a miscible fluid, Europhys. Lett. **9**, 333 (1989).
[5] F. T. Arecchi, P. K. Buah-Bassuah, and C. Perez-Garcia, Fragment formation in the break-up of a drop falling in a miscible liquid, Europhys. Lett. **15**, 429 (1991).
[6] F. T. Arecchi, P. K. Buah-Bassuah, F. Francini, and S. Residori, Fragmentation of a drop as it falls in a lighter miscible fluid, Phys. Rev. E **54**, 424 (1996).
[7] S. Residori, P. K. Buah-Bassuah, and F. T. Arecchi, Fragmentation instabilities of a drop as it falls in a miscible fluid, Eur. Phys. J. Special Topics **146**, 357 (2007).
[8] M. Shimokawa, R. Mayumi, T. Nakamura, T. Toshiya, and H. Sakaguchi, Breakup and deformation of a droplet falling in a miscible solution, Phys. Rev. E **93**, 062214 (2016).
[9] W. M. Haynes, *CRC Handbook of Chemistry and Physics*, 94th ed. (CRC Press/Taylor and Francis, Boca Raton, FL, 2014).
[10] T. Bosse, L. Kleiser, J. Favre, and E. Meiburg, Settling and breakup of suspension drops, Phys. Fluids **17**, 091107 (2005).
[11] A. Mylyk, W. Meile, G. Brenn, and M. L. Ekiel-Jezewska, Break-up of suspension drops settling under gravity in a viscous fluid close to a vertical wall, Phys. Fluids **23**, 063302 (2011).
[12] B. Metzger, M. Nicolas, and E. Guazzelli, Falling clouds of particles in viscous fluids, J. Fluid Mech. **580**, 283 (2007).
[13] K. Adachi, S. Kiriyama, and N. Yoshioka, The behavior of a swarm of particles moving in a viscous fluid, Chem. Eng. Sci. **33**, 115 (1978).
[14] J. Park, B. Metzger, E. Guazzelli, and J. E. Butler, A cloud of rigid fibres sedimenting in a viscous fluid, J. Fluid Mech. **648**, 351 (2010).
[15] G. Machu, W. Meile, L. C. Nitsche, and U. Schaflinger, Coalescence, torus formation and breakup of sedimenting drops: Experiments and computer simulations, J. Fluid Mech. **447**, 299 (2001).
[16] M. Kojima, E. J. Hinch, and A. Acrivos, The formation and expansion of a toroidal drop moving in a viscous fluid, Phys. Fluid **27**, 19 (1984).
[17] S. Chandrasekhar, *Hydrodynamics and Hydromagnetic Stability* (Dover, New York, 1981).
[18] S. E. Widnall, D. B. Bliss, and C.-Y. Tsai, The instability of short waves on a vortex ring, J. Fluid Mech. **66**, 35 (1974).
[19] N. Baumann, D. D. Joseph, P. Mohr, and Y. Renardy, Vortex rings of one fluid in another in free fall, Phys. Fluids A **4**, 567 (1992).
[20] S. Residori, E. Pampaloni, P. K. Buah-Bassuah, and F. T. Arecchi, Surface tension effects in the zero gravity inflow of a drop into a fluid, Eur. Phys. J. B **15**, 331 (2000).
[21] P. K. Buah-Bassuah, R. Rojas, S. Residori, and F. T. Arecchi, Fragmentation instability of a liquid drop falling inside a heavier miscible fluid, Phys. Rev. E **72**, 067301 (2005).
[22] T. Naitoh, N. Fukuda, T. Gotoh, H. Yamada, and K. Nakajima, Experimental study of axial flow in a vortex ring, Phys. Fluids **14**, 143 (2002).
[23] Y. Fukumoto and H. K. Moffatt, Motion and expansion of a viscous vortex ring. Part 1. A higher-order asymptotic formula for the velocity, J. Fluid Mech. **417**, 1 (2000).
[24] Y. Fukumoto and F. Kaplanski, Global time evolution of an axisymmetric vortex ring at low Reynolds numbers, Phys. Fluids **20**, 053103 (2008).
[25] P. G. Saffman, The number of waves on unstable vortex rings, J. Fluid Mech. **84**, 625 (1978).
[26] J. S. Turner, Buoyant plumes and thermals, Annu. Rev. Fluid Mech. **1**, 29 (1969).
[27] A range of numerical results, denoted by a solid line, is $3 \lesssim G \lesssim 100$, because the linear relationship between G and α/ν in Fig. 9 is satisfied for $G \gtrsim 3$; i.e., α/ν becomes negative for $G \lesssim 3$ in the linear fitting. Thus, numerical results are obtained only for $G \gtrsim 3$. The linear fitting should be changed into some nonlinear fitting around at $G \sim 3$ to obtain numerical results for $G \lesssim 3$.